

Two-Element Quadrifilar Array

FREDERICK R. DOMER

*Spacecraft Technology Center
Space Science and Technology Area*

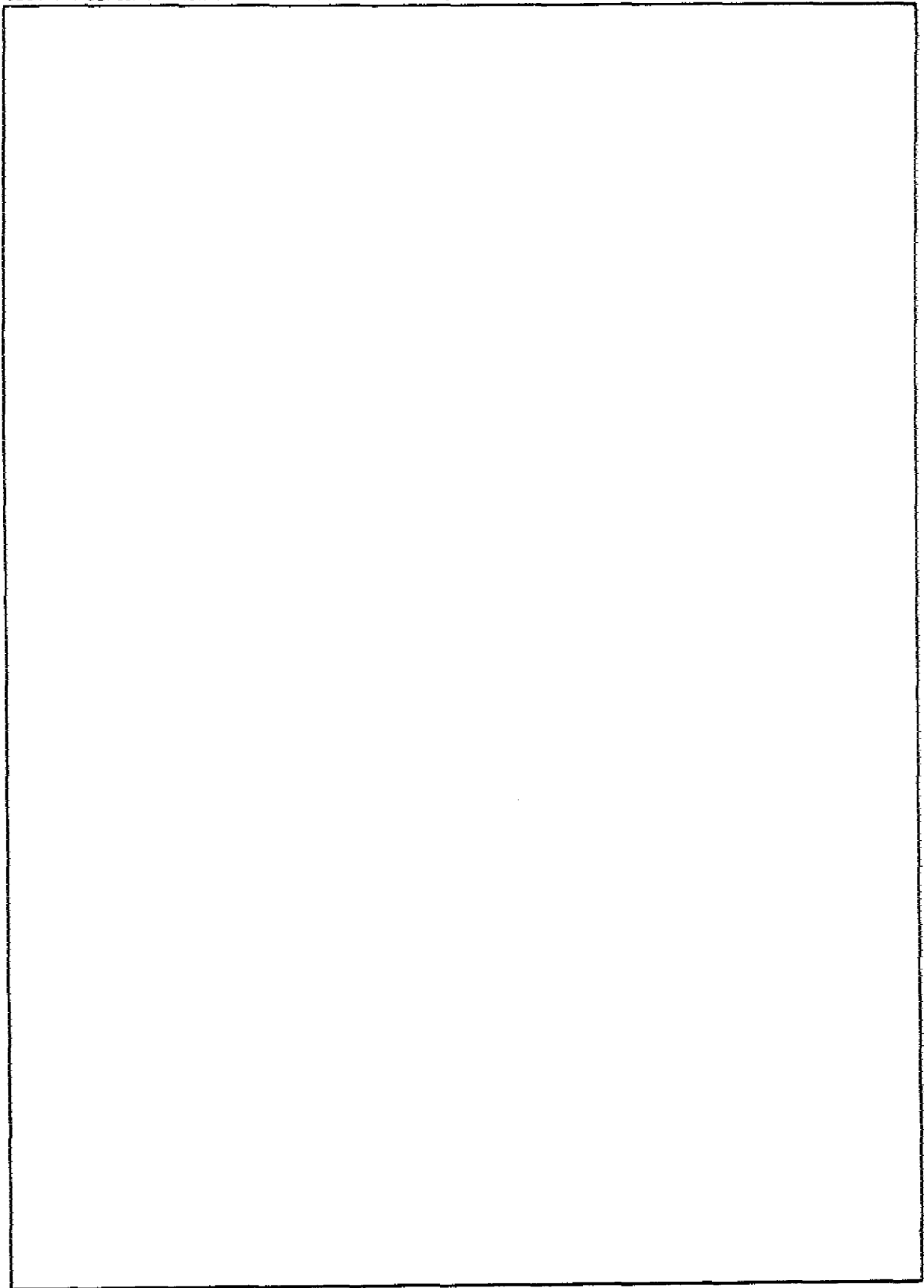
March 8, 1974



NAVAL RESEARCH LABORATORY
Washington, D.C.

Approved for public release; distribution unlimited.

REPORT DOCUMENTATION PAGE		READ INSTRUCTIONS BEFORE COMPLETING FORM
1. REPORT NUMBER NRL Report 7671	2. GOVT ACCESSION NO.	3. RECIPIENT'S CATALOG NUMBER
4. TITLE (and Subtitle) Two-Element Quadrifilar Array		5. TYPE OF REPORT & PERIOD COVERED
7. AUTHOR(s) Frederick R. Domer		6. PERFORMING ORG. REPORT NUMBER
9. PERFORMING ORGANIZATION NAME AND ADDRESS Naval Research Laboratory Washington, D.C. 20375		8. CONTRACT OR GRANT NUMBER(s)
11. CONTROLLING OFFICE NAME AND ADDRESS Department of the Navy Office of Naval Research Arlington, Va. 22217		10. PROGRAM ELEMENT, PROJECT, TASK AREA & WORK UNIT NUMBERS NRL Problem A01-17
14. MONITORING AGENCY NAME & ADDRESS (If different from Controlling Office)		12. REPORT DATE March 8, 1974
		13. NUMBER OF PAGES 18
		15. SECURITY CLASS. (of this report) Unclassified
		15a. DECLASSIFICATION/DOWNGRADING SCHEDULE
16. DISTRIBUTION STATEMENT (of this Report) Approved for public release; distribution unlimited		
17. DISTRIBUTION STATEMENT (of the abstract entered in Block 20, if different from Report)		
18. SUPPLEMENTARY NOTES		
19. KEY WORDS (Continue on reverse side if necessary and identify by block number) Antenna arrays Helical antennas Spacecraft tracking		
20. ABSTRACT (Continue on reverse side if necessary and identify by block number) Several quadrifilar helices were built and tested, and a three-quarter-turn, quadrifilar helix was selected for use in a two-element vertical array as a fixed satellite ground antenna. A vertical array of two of the helices was then designed and tested. The pattern provides hemisphere coverage and has a fairly sharp cutoff at the horizon to reduce multipath effects. Impedance measurements, polar patterns, and radiation distribution plots of axial ratio, tilt angle, and polarization loss further verify that this antenna is applicable to satellite tracking.		



CONTENTS

INTRODUCTION	1
SINGLE QUADRIFILAR HELIX	1
QUADRIFILAR ARRAY	3
ACKNOWLEDGMENT	15
REFERENCES	15

TWO-ELEMENT QUADRIFILAR ARRAY

INTRODUCTION

Two desirable properties of a satellite-tracking antenna are hemisphere coverage and rejection of unwanted signals such as multipath. If the ground antenna is steerable, these properties are achieved by virtue of a narrow beamwidth. However, if the antenna is fixed, a wide beamwidth is required for hemisphere coverage, and a sharp pattern cutoff at the horizon is desirable to reduce multipath effects. To achieve both these requirements, an array of two quadrifilar helices with the proper phasing and spacing was designed.

Measurements were made in an anechoic chamber which has recently been instrumented with a computer and magnetic tape system. Computer programs were written to compute axial ratio, tilt angle, and polarization loss and were applied to the quadrifilar array.

SINGLE QUADRIFILAR HELIX

The multifilar helix excited with a progressive phase relationship was first examined by Gerst [1]. The quadrifilar helix consists of four identical windings rotated 90° apart and fed with a $0^\circ, 90^\circ, 180^\circ, 270^\circ$ phase relationship. As is true with the single-winding helix, if the quadrifilar helix has several turns, it becomes a traveling-wave antenna; however a quadrifilar with one turn or less is a resonant structure [2, 3].

Several quadrifilar helices were built and tested. Figure 1 shows the case selected for the array which will be discussed in the next section. The preliminary quadrifilar models were constructed of copper tape wound on a styrofoam cylinder. The antenna is fed from the top, with a balun through the center of the cylinder and a hybrid at the base. This excited the four windings with the necessary 90° phase progression. The tests were conducted at the bottom of the UHF band.

The three-quarter-turn quadrifilar helix of Fig. 1 is $0.63\lambda_0$ in length (λ_0 at the center frequency, designated), f_R , and $0.11\lambda_0$ in diameter. The copper-tape windings have a width of $0.02\lambda_0$ and are $0.71\lambda_0$ long. A Smith-chart plot of impedance is shown in Fig. 2. Unlike the traveling-wave quadrifilar, the short resonant quadrifilar helix is narrow-band, exhibiting about a 4% impedance bandwidth ($VSWR < 2$) for this case. However the the resonant resistance for this quadrifilar helix is a convenient 50Ω , obviating the need for any matching transformers.

A polar pattern for circular polarization is shown in Fig. 3. The zenith corresponds to $\theta = 0$ (north pole of a spherical coordinate system), considering the quadrifilar helix

Note: Manuscript submitted October 10, 1973.

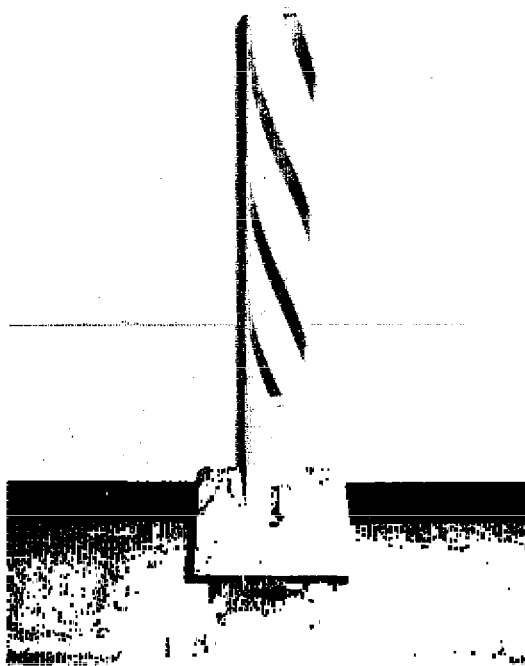


Fig. 1—Three-quarter-turn quadrifilar helix

as a ground antenna. The axial ratio is in general low, with a maximum in the north-pole hemisphere of approximately 4 dB. Good circularity throughout the hemisphere is important for satellite tracking, since the satellite antenna will often have high axial ratios over part of the pattern or could even be a linear antenna. Faraday-rotation effects prevent the determination of the arriving wave polarization from a linear satellite antenna at VHF and UHF frequencies.

Although the pattern of Fig. 3 provides good hemisphere coverage, it decreases rather slowly for $\theta > 90^\circ$. This slow pattern cutoff below the horizon, inherent with the resonant quadrifilar helix because of the short length, leads to poor multipath rejection. Figure 4 illustrates direct and ground-reflected signals arriving at the antenna. For grazing incidence (α small) the magnitude of ground reflection coefficients are near 1.0 for $E\phi$ or $E\theta$ polarization. The reflection coefficient for $E\phi$ polarization remains large for most angles of incidence. Consider $\theta = 85^\circ$ ($\alpha = 5^\circ$): the polarization is $E\phi$, and the ground reflection coefficient is 0.95. The pattern in Fig. 3 is for circular polarization; however $E\phi$ and $E\theta$ patterns are similar. Therefore, the multipath rejection due to the pattern is only 2 dB ($\theta = 85^\circ$ and $\theta = 95^\circ$). This could lead to fading in which the sum of the direct and reflected signal would be 12dB below the direct signal alone. Multipath effects are the most severe near the horizon, when the path loss to the satellite is also maximum. Multipath effects may be difficult to determine, for example, if the antenna was on the edge of a roof and the ground was not level. Thus an antenna which has better multipath rejection would be advantageous.

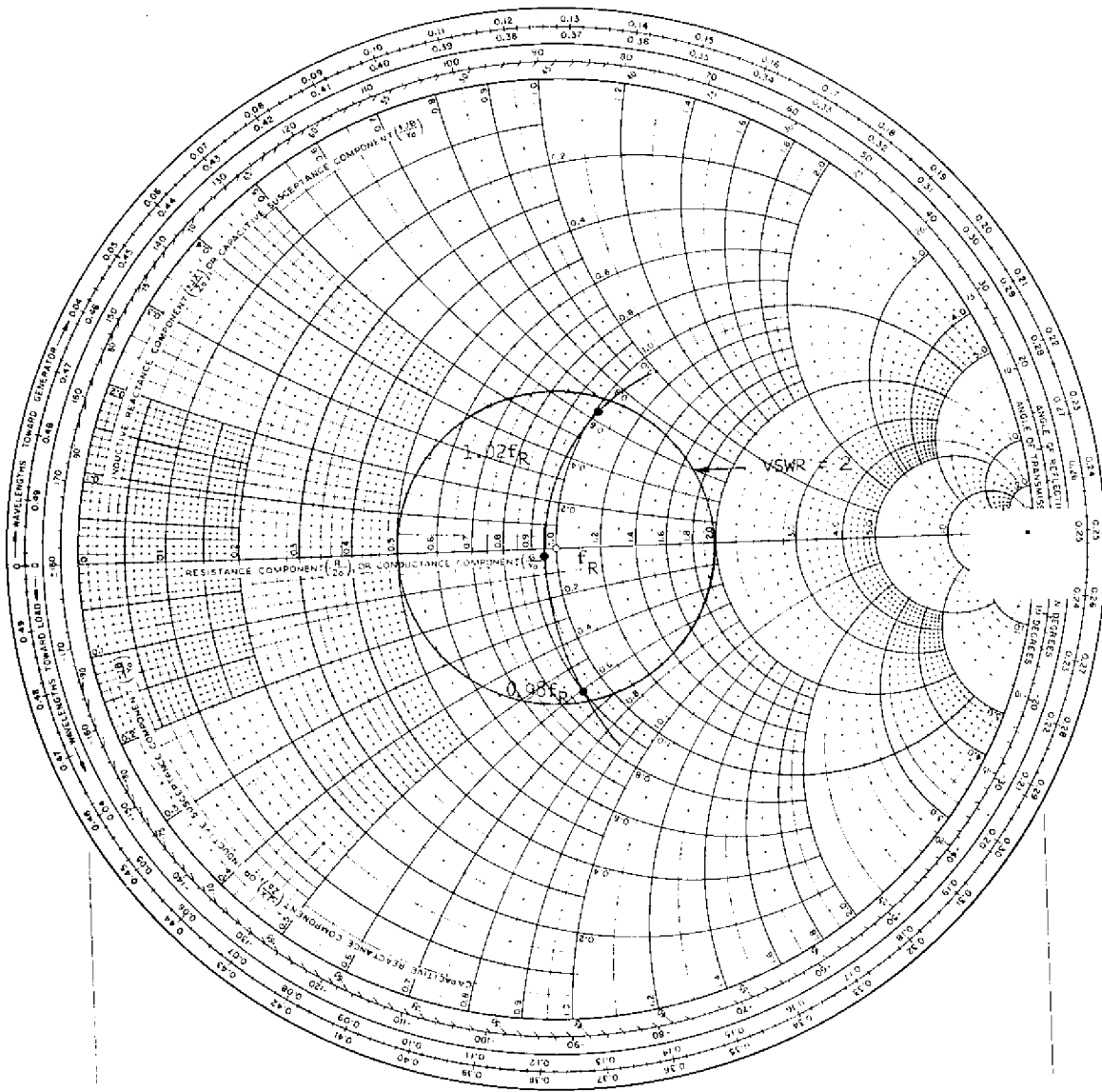


Fig. 2—Impedance bandwidth of the quadrifilar helix shown in Fig. 1

QUADRIFILAR ARRAY

An array of two quadrifilar helices will be discussed next. This array is an attempt to achieve the necessary hemispherical coverage for fixed satellite tracking while having a sharp pattern cutoff at the horizon to reduce multipath effects. A vertical array was chosen, since it will be omnidirectional in ϕ , provide pattern control, and make possible a sharper cutoff at the horizon because of the increased length.

The separation, relative phase, and element pattern determine the array pattern. We first consider an array of two omnidirectional sources (Fig. 5) with separation d and relative phase γ . The received signal due to a plane wave is

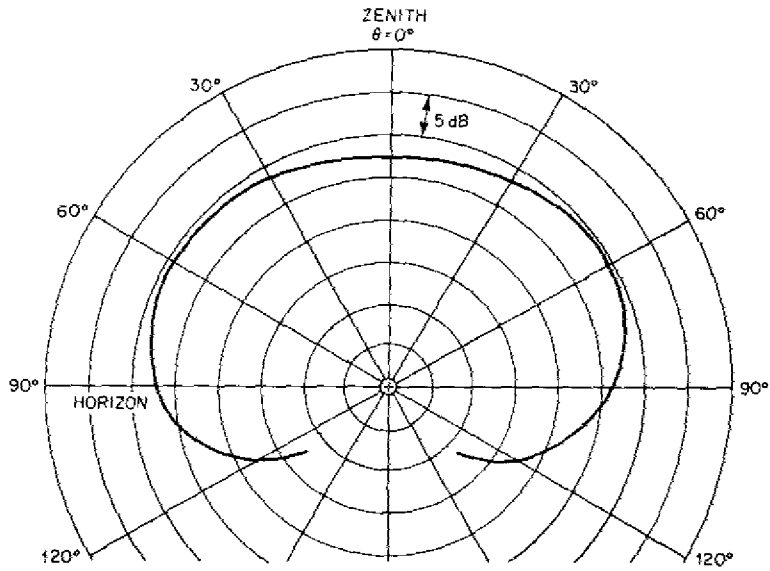


Fig. 3—Typical θ cut for the quadrifilar helix (Fig. 1) measured using circular polarization

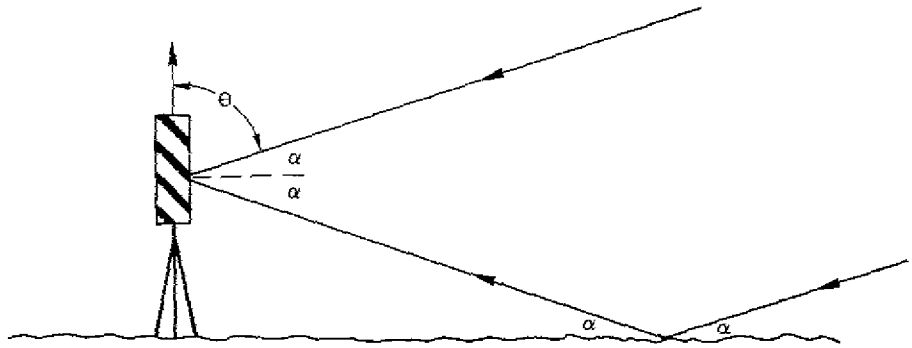


Fig. 4—Quadrifilar ground antenna with multipath interference

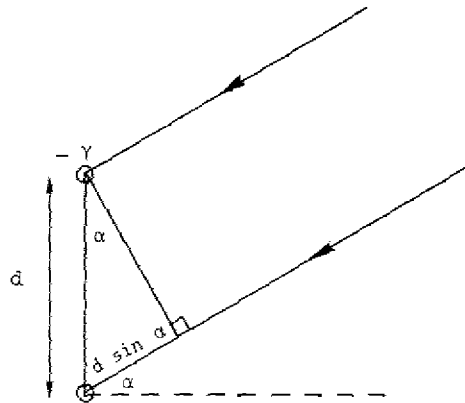


Fig. 5—Array of two omnidirectional sources

$$R e^{j\phi_R} = e^{-j\gamma} + e^{-j(2\pi d \sin \alpha)/\lambda_0}, \quad (1)$$

where R and ϕ_R are the received amplitude and phase. Only the amplitude R is of interest, with the maximum amplitude being 2 from Eq. (1). Normalizing and expanding Eq. (1), we get

$$\frac{R}{2} = \sqrt{\frac{1 + \cos\left(\gamma - \frac{2\pi d \sin \alpha}{\lambda_0}\right)}{2}} \quad (2)$$

In terms of dB level the amplitude pattern becomes

$$\text{dB} = 10 \log_{10} \left[\frac{1 + \cos\left(\gamma - \frac{2\pi d \sin \alpha}{\lambda_0}\right)}{2} \right] \quad (3)$$

We now consider the case in which the array pattern at zenith ($\alpha = 90^\circ$) is 15 dB below the peak of the pattern. Gain requirements for a satellite ground antenna are usually less severe overhead because the path loss is minimum, satellite antenna gain is at the peak, and the signal has already been acquired. Then from Eq. (2)

$$0.178 = \sqrt{\frac{1 + \cos\left(\gamma - \frac{2\pi d}{\lambda_0}\right)}{2}}, \quad (4)$$

which gives the following relationship between the separation and phasing:

$$\gamma = 360d/\lambda_0 - 159.5. \quad (5)$$

The worst-case multipath effects normally occur at the minimum elevation angles. For example, if tracking is limited to $\alpha > 10^\circ$, then the worst-case is near $\alpha = 10^\circ$. We first assume perfect ground reflection and two omni sources; then the signal level from Eq. (2) for out-of-phase multipath is

$$S_1 = \sqrt{\frac{1 + \cos\left(\gamma - \frac{2\pi d \sin 10^\circ}{\lambda_0}\right)}{2}} - \sqrt{\frac{1 + \cos\left(\gamma + \frac{2\pi d \sin 10^\circ}{\lambda_0}\right)}{2}} \quad (6)$$

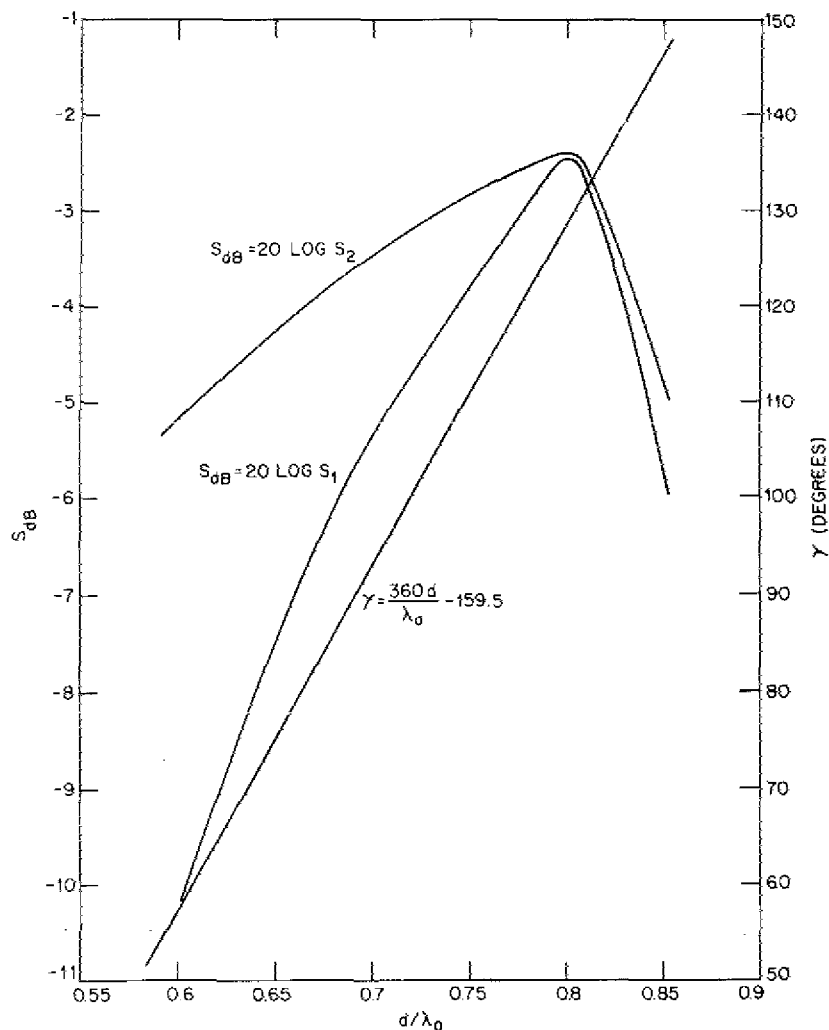


Fig. 6—Plots of Eqs. (5), (7), and (8)

Substituting for γ from Eq. (5), we get

$$S_1 = \sqrt{\frac{1 + \cos\left(\frac{297.5d}{\lambda_0} - 159.5\right)}{2}} - \sqrt{\frac{1 + \cos\left(\frac{422.5d}{\lambda_0} - 159.5\right)}{2}} \quad (7)$$

The dB level of S_1 ($S_{dB} = 20 \log S_1$) is plotted against d/λ_0 in Fig. 6 along with Eq. (5). The signal level as a function of d/λ_0 depends on both the direct gain at $\alpha = +10^\circ$ and the reflected gain at $\alpha = -10^\circ$ and represents the dB level relative to the peak gain with no reflection. If we assume a reflection coefficient of 0.9 and a 3-dB element pattern rejection ($\alpha = -10^\circ$ relative to $\alpha = +10^\circ$), the level for out-of-phase multipaths is

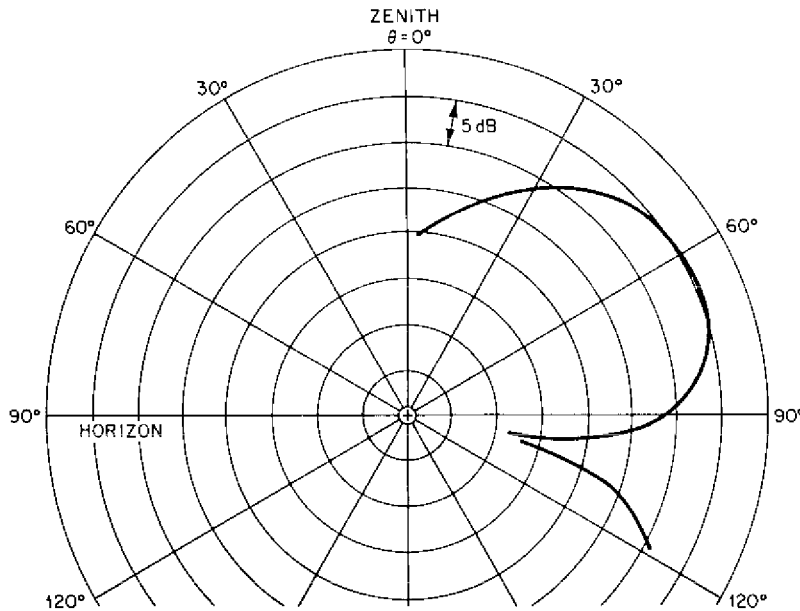


Fig. 7—Pattern for an array of two isotropic sources with $d/\lambda_0 = 0.78$ and $\gamma = 120^\circ$

$$S_2 = \sqrt{\frac{1 + \cos\left(\frac{297.5d}{\lambda_0} - 159.5\right)}{2}} - 0.637 \sqrt{\frac{1 + \cos\left(\frac{422.5d}{\lambda_0} - 159.5\right)}{2}}, \quad (8)$$

which is plotted in Fig. 6. For both cases the optimum d/λ_0 is near 0.8; however because of the rapid decrease in level for $d/\lambda_0 > 0.8$ a value of $d/\lambda_0 = 0.78$ was chosen. This case is plotted in Fig. 7 with $\gamma = 120^\circ$. The gain at zenith is approximately -15 dB with respect to the peak, and the pattern decreases rapidly below the horizon due to the null near $\alpha = -10^\circ$. Reduction of the backlobe will depend on the element pattern.

The balun for the vertical array (Fig. 8) is constructed of semirigid coax. Both antennas can be connected to the same structure because of the $\lambda_0/4$ short between the individual antenna baluns. The relative phase is determined by the 0.78λ separation (λ being the wavelength in the semirigid coax), the 180° difference between the two individual baluns, and the phasing network composed of three 90° hybrids.

The three-quarter-turn quadrifilar helix (Fig. 1) was used for the two elements of the array (Fig. 9). Impedance measurements at the four inputs were identical and exhibited almost no change from the previous measurements (Fig. 2) on the single quadrifilar helix. Thus with the effect of mutual coupling small, pattern calculations combining the array factor and element pattern should be fairly accurate. A typical θ cut for the quadrifilar array measured with left-hand circular polarization is shown in Fig. 10 with the isotropic level near 8. Calculated values based upon the element pattern of Fig. 3 and the array factor of Fig. 7 are also plotted. The calculated points were normalized to the peak of the measured pattern and show good agreement.

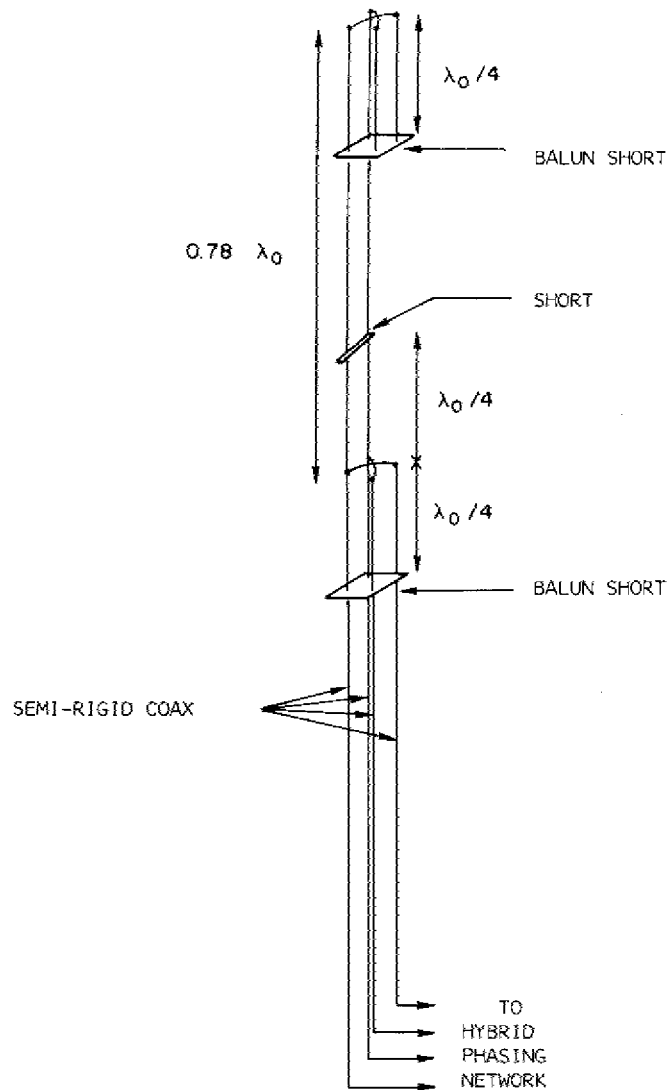


Fig. 8—Balun for a vertical array of two quadrifilar helices

A quadrifilar array for outside use was constructed of aluminum tubing and nylon containing a light stabilizer. The antenna is shown in Fig. 11 mounted on the dielectric head in the anechoic chamber. A radiation distribution plot for left-hand circular polarization is shown in Fig. 12. The directivity isotropic level is 9.6 dB; numbers less than 9.6 are above isotropic. The rapid decrease in signal level for $\theta > 90^\circ$ is evident. The level of right-hand circular polarization is low for all θ .

The anechoic chamber is instrumented with a computer and magnetic tape system. Two amplitudes and the phase angle between these amplitudes are measured at each $\theta\phi$ coordinate and stored on magnetic tape. Usually the amplitudes correspond to E_θ and E_ϕ . Computer programs were written to compute other antenna properties such as axial ratio, tilt angle, and polarization loss from the data stored on magnetic tape.

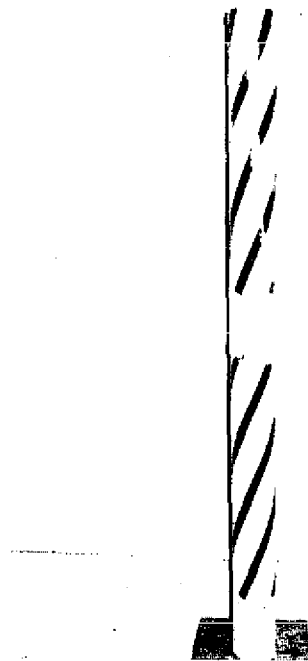


Fig. 9—Vertical array of two quadrifilar helices

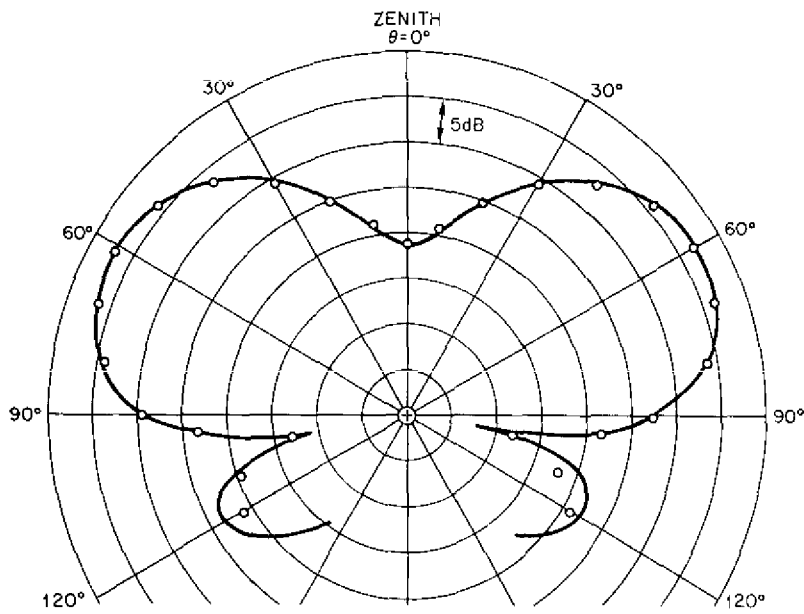


Fig. 10—Typical θ cut for the quadrifilar array (Fig. 9) measured using circular polarization. The calculated points are normalized to the peak of the measured pattern.



Fig. 11—Quadrifilar array made for outside use by substituting aluminum tubing for the copper-tape windings on styrofoam shown in Fig. 9

Axial ratio can be expressed in terms of right- and left-hand circular polarization components as

$$\text{axial ratio} = \frac{E_{RHC} + E_{LHC}}{|E_{RHC} - E_{LHC}|}, \quad (9)$$

where E_{RHC} and E_{LHC} are determined by

$$E_{RHC} = \sqrt{\frac{E_{\theta}^2 + E_{\phi}^2 + 2E_{\theta}E_{\phi} \sin \delta}{2}} \quad (10)$$

and

$$E_{LHC} = \sqrt{\frac{E_{\theta}^2 + E_{\phi}^2 - 2E_{\theta}E_{\phi} \sin \delta}{2}} \quad (11)$$

and δ is the phase angle of E_{ϕ} relative to E_{θ} . The dB axial ratio for the quadrifilar array is shown in Fig. 13. From 5° elevation angle to overhead the maximum axial ratio is 4 dB and the ratio is usually much lower.

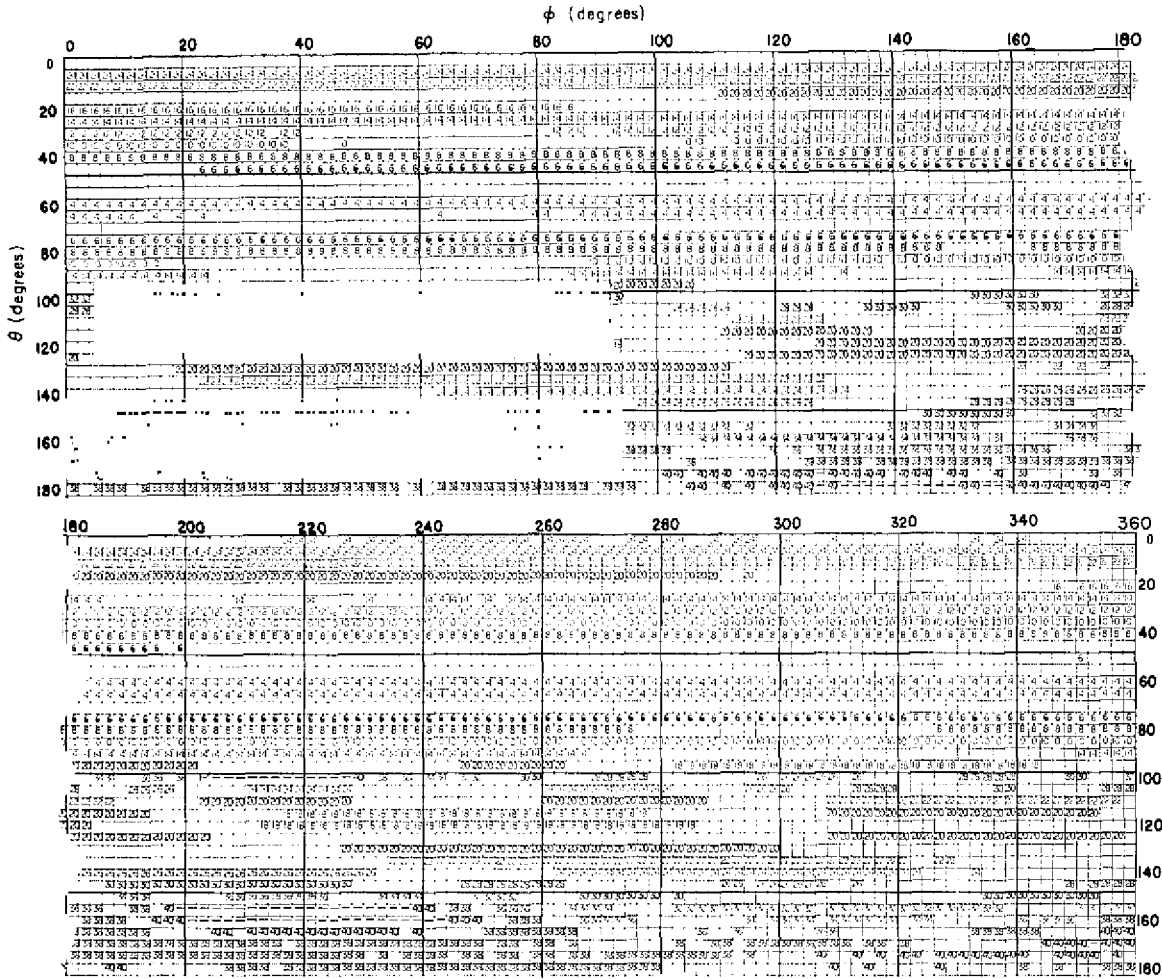


Fig. 12—Radiation pattern of the quadrifilar array shown in Fig. 11 measured using left-hand circular polarization

The polarization ellipse tilt angle is given by

$$\text{tilt angle} = \frac{1}{2} \tan^{-1} \left(\frac{2E_{\theta} E_{\phi} \cos \delta}{E_{\theta}^2 - E_{\phi}^2} \right). \quad (12)$$

The tilt angle is measured counterclockwise from the E_{θ} axis (90° corresponds to the E_{ϕ} direction). The tilt angle pattern for the array is shown in Fig. 14. The numbers must be multiplied by 5 to obtain the actual angle; thus 0 and 36 correspond to the ellipse maximum along E_{θ} , and the number 18 corresponds to the E_{ϕ} direction.

The polarization loss between an antenna with axial ratio R^A and a wave with axial ratio R^W is

FREDERICK R. DOMER

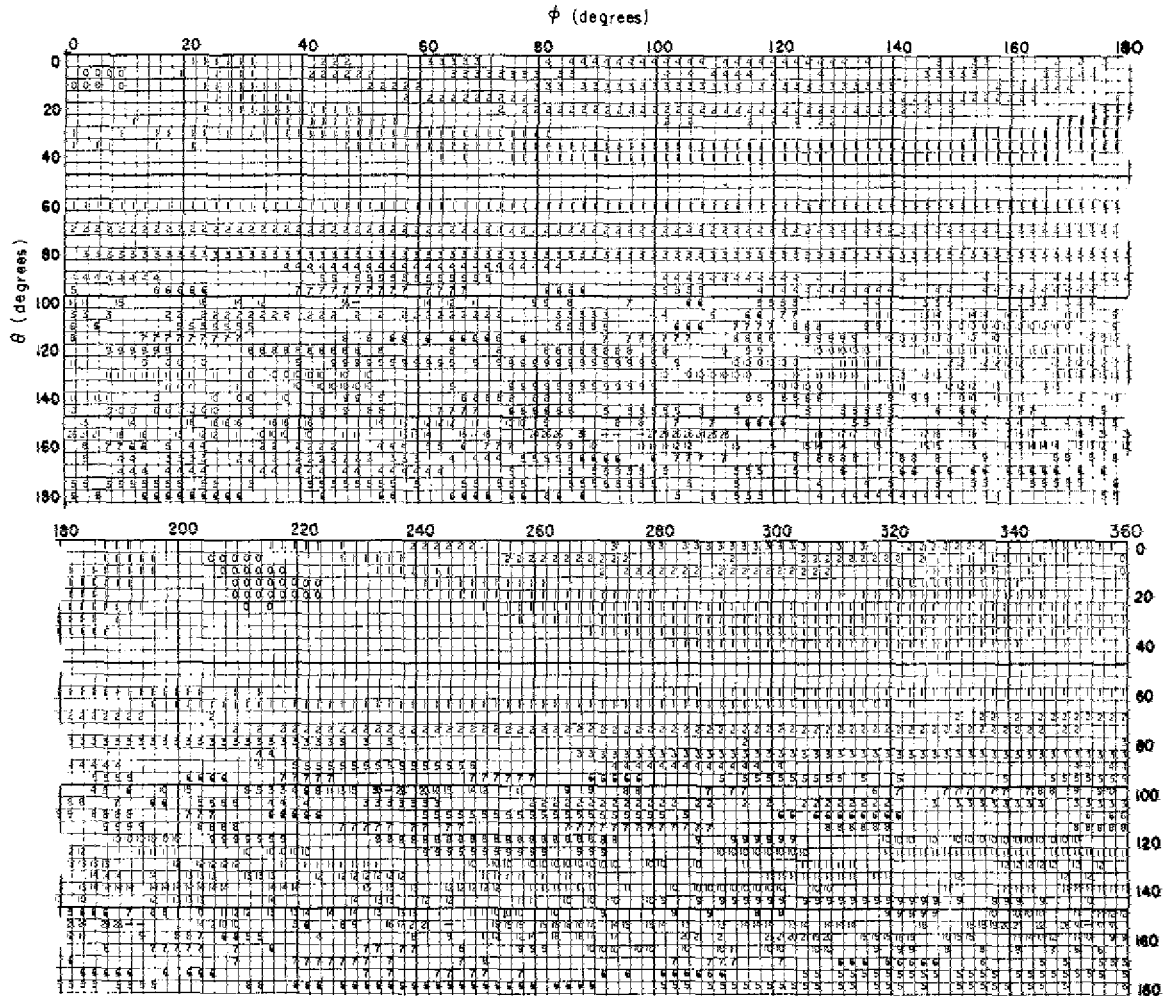


Fig. 13—Radiation pattern of the quadrifilar array shown in Fig. 11 for the axial ratio in dB

$$\text{polarization loss} = \frac{[(R^A)^2 + 1][(R^W)^2 + 1]}{[R^A R^W \pm 1]^2 \cos^2 \tau + [R^A \pm R^W]^2 \sin^2 \tau}, \quad (13)$$

where τ is the tilt angle between the antenna ellipse and the wave ellipse. The plus is used for same-sense rotation and the minus for opposite-sense rotation. The maximum polarization loss occurs when the ellipses are orthogonal ($\tau = 90^\circ$). This case is shown in Fig. 15 for same-sense rotation and three different wave axial ratios incident upon the quadrifilar array.

The distribution plots given in Figs. 12 through 15 thus verify in detail that the quadrifilar array should be a useful satellite-tracking antenna.

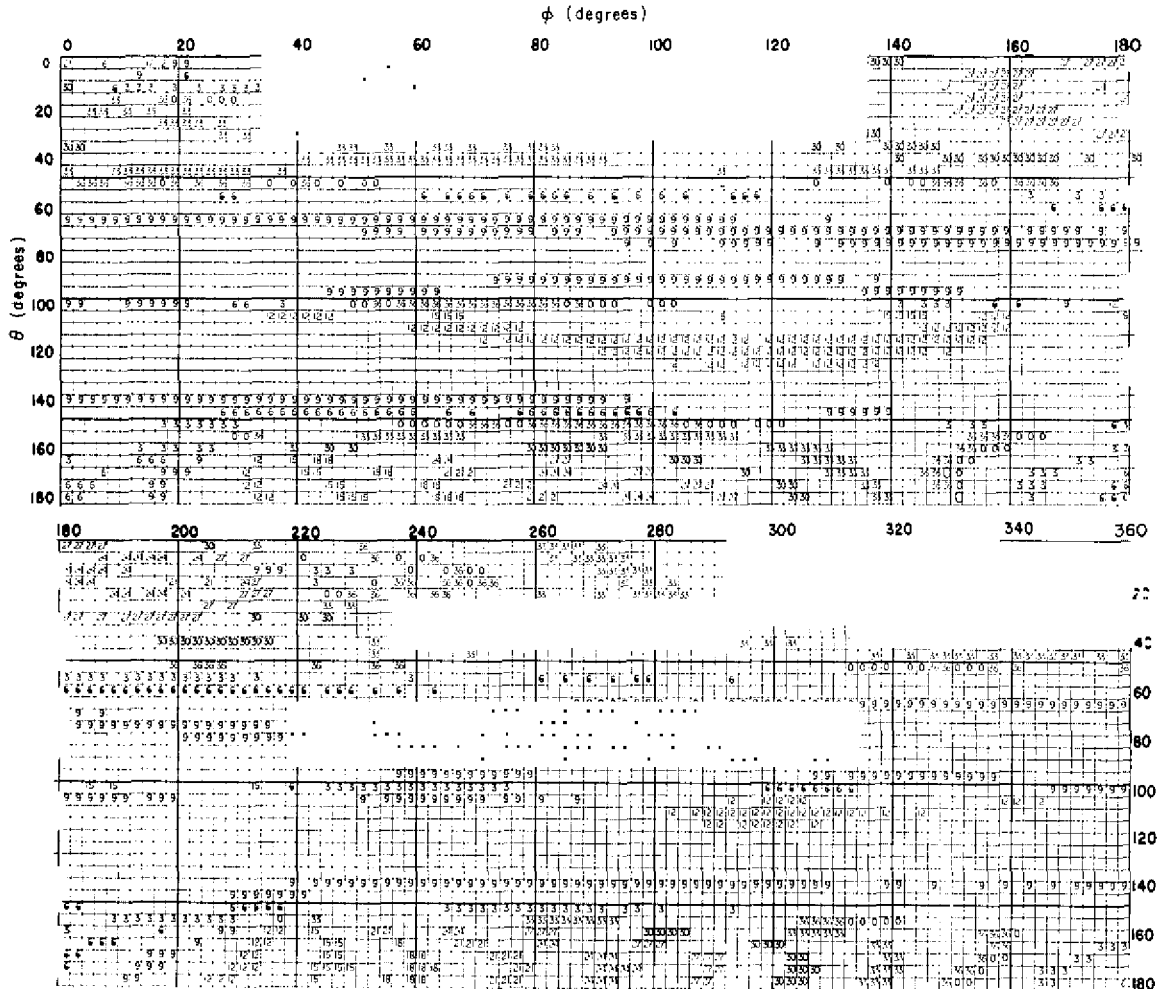
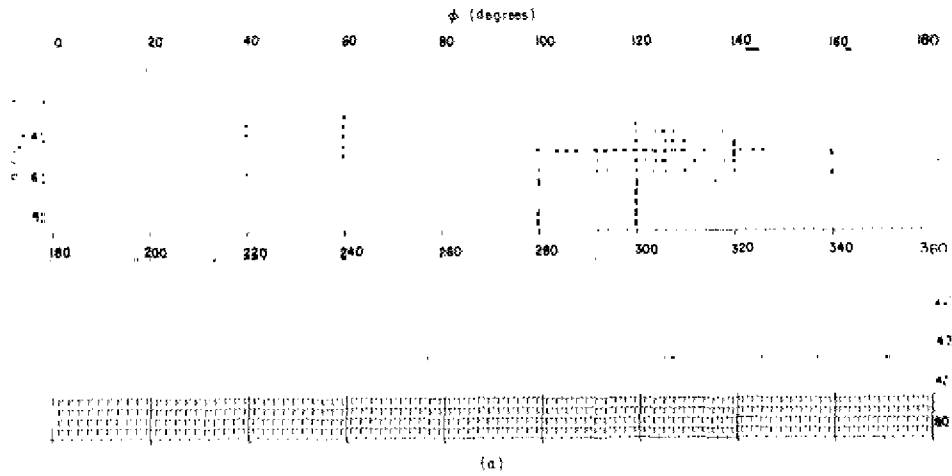
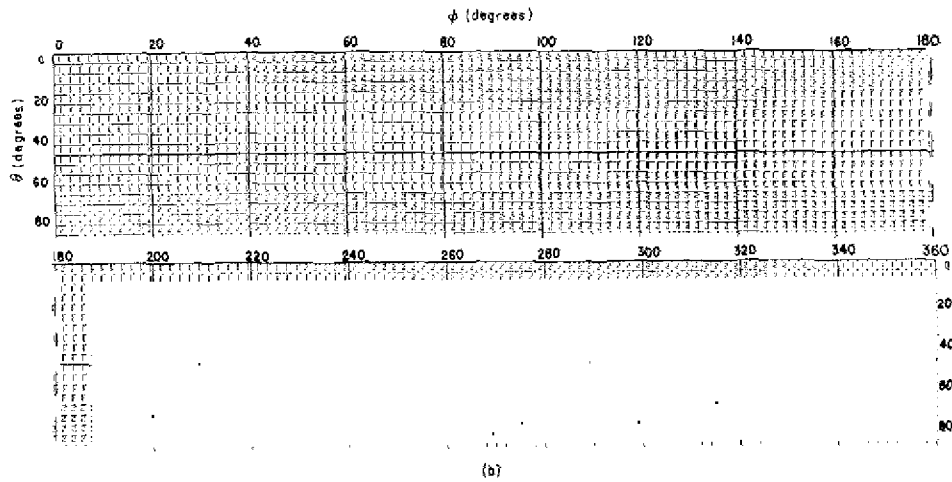


Fig. 14—Radiation pattern of the quadrifilar array shown in Fig. 11 for the polarization ellipse tilt angle. The values must be multiplied by 5 to obtain the actual angle.

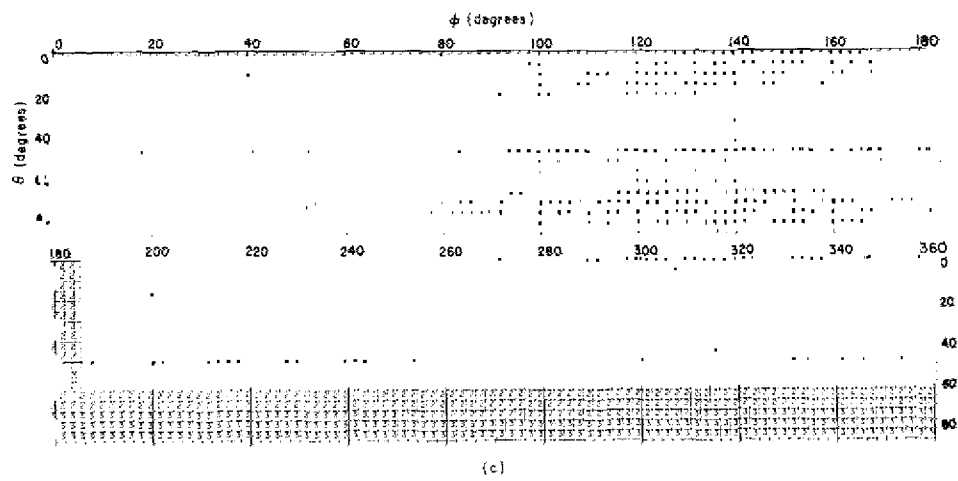
FREDERICK R. DOMER



(a) Axial ratio = 5 dB



(b) Axial ratio = 10 dB



(c) Axial ratio = 15 dB

Fig. 15—Radiation pattern of the quadrifilar array shown in Fig. 11 for the worst case of polarization loss with same-sense rotation

ACKNOWLEDGMENT

I acknowledge the assistance of Henry J. Rogers, who contributed to the mechanical design and building of the quadrifilar array.

REFERENCES

1. C. W. Gerst and R. A. Worden, "Helix Antennas Take Turn for Better," *Electronics* 39 (No. 17), 100-110 (Aug. 22, 1966).
2. C. C. Kilgus, "Resonant Quadrifilar Helix Design," *Microwave Journal* 13 (No. 12), 49-54 (Dec. 1970).
3. H. A. Wheeler, "A Helical Antenna for Circular Polarization," *Proceedings I.R.E.* 35, 1479-1484 (Dec. 1947).
4. E. C. Jordan, *Electromagnetic Waves and Radiating Systems*, Englewood Cliffs, N. J., Prentice-Hall, 2nd edition, 1967.